PHYSICAL REVIEW D **83,** 074002 (2011)

Hadronic production of a MSSM Higgs boson with a pair of stops at the LHC

Hisham A. El-Kolaly and Shymaa M. Seif
Cairo University, Faculty of Science, Physics Department, Giza, Egypt
(Received 15 July 2010; published 1 April 2011)

We present the next-to-leading order supersymmetric-QCD corrections to the production of a light neutral minimal supersymmetric standard model Higgs boson with a pair of supersymmetric scalar partners of the top quark at next-to-leading order at the LHC. We study the dependence of the lowest order total cross section on both the renormalization/factorization scale and the Higgs mass in the framework of minimal supergravity, taking the point SPS1a as a benchmark, for the numerical calculations. The renormalization/factorization scale dependence of the lowest order total cross section is strong. Including the next-to-leading order supersymmetric-QCD corrections significantly reduces and stabilizes the dependence of the lowest order total cross section on the renormalization/factorization scale.

DOI: 10.1103/PhysRevD.83.074002 PACS numbers: 13.85.−t, 14.80.Da

I. INTRODUCTION

One of the major objectives of future high-energy experiments is to search for scalar Higgs particles and investigate the symmetry breaking mechanism of the electroweak interactions. In the standard model (SM) [1], one doublet of complex scalar fields is introduced to spontaneously break the symmetry, leading to a single neutral Higgs boson. But there exists the problem of the quadratically divergent contributions to the corrections to the Higgs boson mass. One of the hopeful models which can solve this problem is the supersymmetric (SUSY) extension to the SM. In this extension model, the quadratic divergences of the Higgs boson mass can be canceled by loop diagrams involving the supersymmetric partners of the SM particles exactly. The most attractive and simplest supersymmetric extension of the SM is the minimal supersymmetric standard model (MSSM)[2,3]. In this model, the Higgs sector consists of three neutral Higgs bosons, one CP-odd particle (A^0), two CP-even particles (h and H), and a pair of charged Higgs bosons ($H^{\pm}$). Supersymmetry predicts the existence of scalar partners $\tilde{f}_L$, $\tilde{f}_R$ to each SM chiral fermion, which mix to produce two mass eigenstates $\tilde{f}_1$ and $\tilde{f}_2$, and spin-$1/2$ partners to the gauge bosons and to the scalar Higgs bosons. In the MSSM, the genuine SUSY particles, neutralino/charginos, and sfermions could have masses not too far from the electroweak symmetry breaking scale. In particular, the lightest neutralino, which is expected to be the lightest SUSY particle (LSP), could have a mass in the range of $\sim$100 GeV. Another particle which could also be light is one of the spin-zero partners of the top quark, the lightest stop $\tilde{t}_1$. Indeed, because of the large m_t value, the two current stop eigenstates could strongly mix [4], leading to a mass eigenstate $\tilde{t}_1$ much lighter than the other squarks (which are constrained to be rather heavy [5] by the negative searches at the Tevatron) and even lighter than the top quark itself. Similar features can also occur in the sbottom sector. These particles could therefore also be easily accessible at the next generation of hadron colliders.

In this paper we study the production of neutral Higgs particles in association with a stop pair at the LHC in the MSSM assuming a minimal supergravity (mSUGRA) symmetry breaking scheme. Theoretical predictions are improved by calculations of the next-to-leading order (NLO) SUSY-QCD corrections with the final-state squarks restricted to $\tilde{t}_1$. This paper proceeds as follows. In Sec. II we present the calculations of the leading order cross sections. We also introduce some basic notations used throughout the paper. In Sec. III we present the calculations of the NLO SUSY-QCD corrections. The contributions are classified into virtual and real corrections with the treatment of soft and collinear singularities. The numerical results and discussions are presented in Sec. IV. Finally, a short conclusion is given.

II. LOWEST ORDER CROSS SECTIONS

The associated production of Higgs bosons with scalar quark pairs has been studied in [6,7]. The cross sections for the production of squarks in association with Higgs bosons in hadron collisions have already been calculated at LO quite some time ago [8,9]. The production mechanism at the parton level contributing to the hadronic process $pp \to \tilde{t}_1\bar{\tilde{t}}_1 h$ involves $q\bar{q}$ annihilation and gluon-gluon fusion channels

$$q(p_1) + \bar{q}(p_2) \to \tilde{t}_1(p_3) + \bar{\tilde{t}}_1(p_4) + h(p_5), \qquad (1)$$

$$g(p_1) + g(p_2) \to \tilde{t}_1(p_3) + \bar{\tilde{t}}_1(p_4) + h(p_5), \qquad (2)$$

where p_1, p_2 and p_3, p_4, p_5 are the four-momenta of the incoming partons and the outgoing particles, respectively. The Feynman diagrams of these subprocesses are plotted in Figs. 1 and 2 respectively.

According to the different topologies of Feynman diagrams, it is convenient to rearrange the amplitudes in terms of their color structure. Therefore, for the subprocess

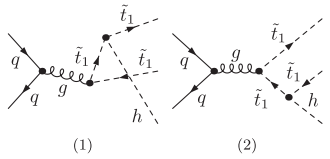

FIG. 1. The LO Feynman diagrams for the $q\bar{q} \to \tilde{t}_1\bar{\tilde{t}}_1 h$ subprocess.

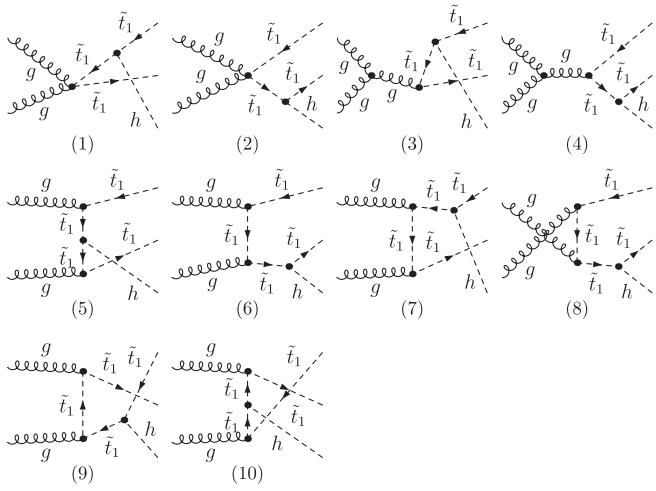

FIG. 2. The LO Feynman diagrams for the $gg \to \tilde{t}_1\bar{\tilde{t}}_1 h$ subprocess.

$q\bar{q} \to \tilde{t}_1\bar{\tilde{t}}_1 h$ the corresponding LO and NLO amplitudes can be expressed in the form

$$\mathcal{M}^{q\bar{q}}_{\mathrm{LO,NLO}} = C^{q\bar{q}}\mathcal{A}^{q\bar{q}}_{\mathrm{LO,NLO}}, \tag{3}$$

where $C^{q\bar{q}}$ is the only color factor involved in the LO amplitude, which can be written as

$$C^{q\bar{q}} = \lambda^c \otimes \lambda^c. \tag{4}$$

The first 3×3 $SU(3)$ Gell-Mann matrix λ^c arises from the $q\bar{q}$ color state, and the second Gell-Mann matrix λ^c arises from the $\tilde{t}_1\bar{\tilde{t}}_1$ color state. Similarly, the LO amplitude of the subprocess $gg \to \tilde{t}_1\bar{\tilde{t}}_1 h$ can be expressed as

$$\begin{aligned}\mathcal{M}^{gg}_{\mathrm{LO}} = &(\tfrac{2}{3}C^{gg}_1 + C^{gg}_2 + C^{gg}_3)\mathcal{M}^{gg}_1 \\ &+ (\tfrac{2}{3}C^{gg}_1 - C^{gg}_2 + C^{gg}_3)\mathcal{M}^{gg}_2,\end{aligned} \tag{5}$$

with

$$C^{gg}_1 = \delta^{c_1c_2}\mathbf{1}, \quad C^{gg}_2 = if^{c_1c_2c}\lambda^c, \quad C^{gg}_3 = d^{c_1c_2c}\lambda^c, \tag{6}$$

$$\mathcal{M}^{gg}_1 = \mathcal{M}^{gg}_{\hat{q}} + \tfrac{1}{2}\mathcal{M}^{gg}_{\hat{s}} + \mathcal{M}^{gg}_{\hat{t}}, \tag{7}$$

$$\mathcal{M}^{gg}_2 = \mathcal{M}^{gg}_{\hat{q}} - \tfrac{1}{2}\mathcal{M}^{gg}_{\hat{s}} + \mathcal{M}^{gg}_{\hat{u}}, \tag{8}$$

where $c_n (n = 1, 2)$ are the color indices of incoming gluons, f^{abc} and d^{abc} are the $SU(3)$ antisymmetric and symmetric structure constants, respectively, and matrices $\mathbf{1}$ and λ^c arise from the $\tilde{t}_1\bar{\tilde{t}}_1$ color state. The amplitudes $\mathcal{M}^{gg}_{\hat{q}}$, $\mathcal{M}^{gg}_{\hat{s}}$, $\mathcal{M}^{gg}_{\hat{t}}$, and $\mathcal{M}^{gg}_{\hat{u}}$ represent the quartic channel, s channel, t channel, and u channel, respectively. These amplitudes are given in terms of the leading order Feynman amplitudes, $\mathcal{M}^{Lo}_i$, $i = 1, \ldots, 10$, corresponding to the Feynman diagrams in Fig. 2, as

$$\begin{aligned}\mathcal{M}^{gg}_{\hat{q}} &= \sum_{i=1}^{2}\mathcal{M}^{\mathrm{LO}}_i, \qquad \mathcal{M}^{gg}_{\hat{s}} = \sum_{i=3}^{4}\mathcal{M}^{\mathrm{LO}}_i, \\ \mathcal{M}^{gg}_{\hat{t}} &= \sum_{i=5}^{7}\mathcal{M}^{\mathrm{LO}}_i, \qquad \mathcal{M}^{gg}_{\hat{u}} = \sum_{i=8}^{10}\mathcal{M}^{\mathrm{LO}}_i.\end{aligned} \tag{9}$$

The squared amplitude for the LO can be written as

$$\begin{aligned}|\mathcal{M}^{gg}_{\mathrm{LO}}|^2 = &\frac{256}{3}(|\mathcal{M}^{gg}_1|^2 + |\mathcal{M}^{gg}_2|^2) \\ &- \frac{32}{3}\cdot 2\,\mathrm{Re}(\mathcal{M}^{gg\dagger}_1 \cdot \mathcal{M}^{gg}_2).\end{aligned} \tag{10}$$

The lowest order cross sections for the subprocesses $q\bar{q}$, $gg \to \tilde{t}_1\bar{\tilde{t}}_1 h$ in the MSSM are obtained by using the following formula:

$$\begin{aligned}d\sigma^{ij}_{\mathrm{LO}} = &\frac{k^{ij}_{av}}{2\hat{s}(2\pi)^4}\frac{\kappa(s_{34}, m^2_{\tilde{t}_1}, m^2_{\tilde{t}_1})}{8s_{34}}\frac{\kappa(\hat{s}, s_{34}, m^2_h)}{8\hat{s}} \\ &\times \Theta(s_{34} - 4m^2_{\tilde{t}_1})\Theta(\sqrt{\hat{s}} - 2m_{\tilde{t}_1} - m_h) \\ &\times \Theta([\sqrt{\hat{s}} - m_h]^2 - s_{34}) \\ &\times \sum_{\mathrm{spins,colors}}|\mathcal{M}^{ij}_{\mathrm{LO}}|^2 ds_{34} d\Omega^*_t d\cos(\theta^{\mathrm{CM}}_h),\end{aligned} \tag{11}$$

with

$$\hat{s} = (p_1 + p_2)^2, \quad s_{ij} = (p_i + p_j)^2, \quad i, j = 3, 4, 5, \tag{12}$$

and

$$\kappa(x, y, z) = \sqrt{x^2 + y^2 + z^2 - 2xy - 2xz - 2yz}. \tag{13}$$

The labels ij indicate the specific initial state of the partonic process. The factor k^{ab}_{av} results from the average over the initial-state spins and colors. The LO total cross section of $pp \to \tilde{t}_1\bar{\tilde{t}}_1 h$ can be expressed as

$$\sigma_{\mathrm{LO}} = \sum_{ij}\int dx_1 dx_2 \mathcal{F}^p_i(x_1, \mu)\mathcal{F}^p_j(x_2, \mu)\hat{\sigma}^{ij}_{\mathrm{LO}}, \tag{14}$$

where the $\mathcal{F}^p_i$'s are the LO parton distribution functions (PDF) with parton i in a proton.

III. NLO SUSY-QCD CORRECTIONS

The NLO SUSY-QCD corrections consist of both virtual corrections to the tree-level processes and one-parton real radiation from both the initial and final states. The NLO SUSY-QCD partonic cross section reads

$$\hat{\sigma}_{ij}^{\mathrm{NLO}} = \hat{\sigma}_{ij}^{\mathrm{LO}} + \delta\hat{\sigma}_{ij}^{\mathrm{NLO}}, \tag{15}$$

where $\hat{\sigma}_{ij}^{\mathrm{LO}}$ denotes the LO partonic cross section and $\delta\hat{\sigma}_{ij}^{\mathrm{NLO}}$ describes the corrections to $\hat{\sigma}_{ij}^{\mathrm{LO}}$. The NLO corrections, $\delta\hat{\sigma}_{ij}^{\mathrm{NLO}}$, receive contributions from $q\bar{q}$, gg, qg, and $\bar{q}g$ initiated processes and can be decomposed in the following way:

$$\begin{aligned}\delta\hat{\sigma}_{ij}^{\mathrm{NLO}} &= \int d(PS_3)\bar{\sum} 2\,\mathrm{Re}(\mathcal{M}_{\mathrm{LO}}^{\dagger}\mathcal{M}_{\mathrm{virt}}) \\ &\quad + \int d(PS_4)\bar{\sum}|\mathcal{M}_{\mathrm{real}}|^2 \\ &\equiv \hat{\sigma}_{ij}^{\mathrm{virt}} + \hat{\sigma}_{ij}^{\mathrm{real}},\end{aligned} \tag{16}$$

where the term integrated over the phase space measure $d(PS_3)$ corresponds to the virtual one-loop corrections with three particles in the final state, while the one integrated over the phase space measure $d(PS_4)$ corresponds to the real tree-level corrections with one additional emitted parton. The sum $\bar{\sum}$ indicates that the corresponding amplitudes squared have been averaged over the initial-state degrees of freedom and summed over the final-state ones.

The calculation of the NLO SUSY-QCD corrections has been performed in the framework of the MSSM. We adopt the 't Hooft-Feynman gauge, and use the dimensional regularization method in $D = 4 - 2\epsilon$ dimensions to isolate UV, IR, and collinear singularities. The masses have been renormalized in the on-shell scheme. Renormalization and factorization are performed in the modified minimal subtraction ($\overline{\mathrm{MS}}$) scheme. The Feynman graphs and the relevant amplitude have been generated by using FEYNARTS [10]. These amplitudes have subsequently been reduced in terms of the standard model extension with the help of MATHEMATICA and FORM [11]. The algebraic output of the calculations has been implemented in the FORTRAN program for numerical evaluation. The phase space integration is implemented by using the Monte Carlo technique. We adopt the definitions of one-loop integral functions as in Ref. [12]. Following standard techniques of one-loop calculations, the tensor integrals are algebraically reduced to scalar integrals. The numerical calculations of the IR-infinite integral functions are implemented by using the methods described in Ref. [13]. The FF package [14] has been used to check some of the IR-finite scalar and tensor integrals.

A. Virtual one-loop corrections

The virtual corrections consist of self-energy, vertex, box, and pentagon diagrams. For the virtual particles inside loops, we use the complete supersymmetric QCD spectrum: gluons, gluinos, all quarks, and all squarks. Self-energy and vertex diagrams contain both IR and UV divergences. Box and pentagon diagrams are ultraviolet finite, but have infrared singularities. The IR poles in the virtual corrections are eventually canceled by analogous singularities in the real corrections to the tree-level cross section. The UV divergences are renormalized by introducing a suitable set of counterterms for the renormalization of the coupling constants and the renormalization of the external wave functions of the gluons, of the light quarks, and of the stop quark. Since Higgs-squark interaction involves the squark mixing angles and the trilinear squark couplings, a counterterm for each of these parameters will be needed. We perform the renormalization programme in the on-shell scheme, where the quark and squark masses are defined as the poles of their respective propagators. The renormalization of the strong gauge coupling constant g_s is carried out in the $\overline{\mathrm{MS}}$ renormalization scheme.

The Feynman rules for the counterterms can be expressed in terms of the field renormalization constants of quarks, squarks, gluons, and gluinos. We express the bare quantities by the renormalized ones,

$$\begin{aligned}&\Psi_{q_a}^{\mathrm{bare}} = \Psi_{q_a}^{\mathrm{ren}}(1 + \tfrac{1}{2}\delta Z_{q_a}), \quad \Phi_{\tilde{Q},a}^{\mathrm{bare}} = \Phi_{\tilde{Q},a}^{\mathrm{ren}}(1 + \tfrac{1}{2}\delta Z_{\tilde{Q},a}), \\ &G_{\mu}^{\mathrm{bare}} = G_{\mu}^{\mathrm{ren}}(1 + \tfrac{1}{2}\delta Z_G), \quad \Psi_{\tilde{g}}^{\mathrm{bare}} = \Psi_{\tilde{g}}^{\mathrm{ren}}(1 + \tfrac{1}{2}\delta Z_{\tilde{g}}),\end{aligned} \tag{17}$$

together with the renormalization constants for the strong coupling, for the strong Yukawa coupling, and for the squark masses, which are defined according to

$$\begin{aligned}g_s^{\mathrm{bare}} &= g_s^{\mathrm{ren}}(1 + \delta Z_g), \\ \hat{g}_s^{\mathrm{bare}} &= \hat{g}_s^{\mathrm{ren}}(1 + \delta Z_{\hat{g}}), \\ m_{\tilde{Q},a}^{2\mathrm{bare}} &= m_{\tilde{Q},a}^{2\mathrm{ren}} + \delta m_{\tilde{Q},a}^2.\end{aligned} \tag{18}$$

The field renormalization constants of the quarks are obtained via the on-shell conditions

$$\begin{aligned}\delta Z_{q_a} = &-\mathrm{Re}\{\Sigma_{q_a}(m_q^2)\} - m_q^2\,\mathrm{Re}\Big\{\frac{\partial}{\partial p^2}(\Sigma_{q_L}(p^2) \\ &+ \Sigma_{q_R}(p^2) + 2\Sigma_{q_S}(p^2))\Big\}_{p^2=m_q^2} (a = L, R),\end{aligned} \tag{19}$$

with the scalar coefficients in the Lorentz decomposition of the self-energy,

$$\Sigma_q(\not{p}) = \not{p}\omega_-\Sigma_{q_L}(p^2) + \not{p}\omega_+\Sigma_{q_R}(p^2) + m_q\Sigma_{q_S}(p^2), \tag{20}$$

and the renormalization constants of the squark sector are fixed by the on-shell conditions

$$\begin{aligned}\delta Z_{\tilde{Q},a} &= -\mathrm{Re}\Big\{\frac{\partial\Sigma_{\tilde{Q},a}(p^2)}{\partial p^2}\Big\}_{|p^2=m_{\tilde{Q},a}^2}, \\ \delta m_{\tilde{Q},a}^2 &= \mathrm{Re}\{\Sigma_{\tilde{Q},a}(m_{\tilde{Q},a}^2)\}.\end{aligned} \tag{21}$$

Also in the gluino sector, we determine the renormalization constants by the on-shell conditions

$$\delta m_{\tilde{g}} = \frac{1}{2}\,\mathrm{Re}\{m_{\tilde{g}}(\Sigma_{\tilde{g}_L}(m_{\tilde{g}}^2) + \Sigma_{\tilde{g}_R}(m_{\tilde{g}}^2) + 2\Sigma_{\tilde{g}_S}(m_{\tilde{g}}^2))\},$$

$$\delta Z_{\tilde{g}} = -\mathrm{Re}\{\Sigma_{\tilde{g}_L}(m_{\tilde{g}}^2)t\} - m_{\tilde{g}}^2\,\mathrm{Re}\Big\{\frac{\partial}{\partial p^2}(\Sigma_{\tilde{g}_L}(p^2) + \Sigma_{\tilde{g}_R}(p^2) + 2\Sigma_{\tilde{g}_S}(p^2)\Big\}_{|p^2=m_{\tilde{g}}^2}. \quad (22)$$

The full set of virtual corrections is UV finite after including the proper counterterms for squark triple and quartic vertices, quark vertices, and self-energies. The actual expressions of the counterterms are

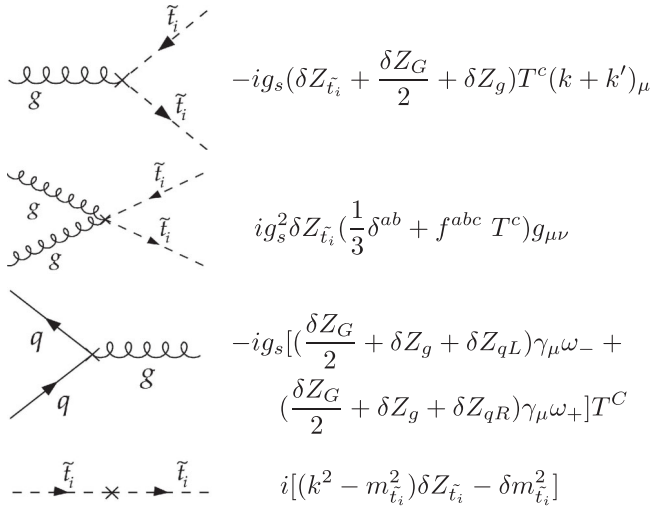

where k, k' denote the momenta of top squarks, a, b, and c are the gluonic color indices, T^c and f^{abc} are the color factors, and $\omega_\pm = (1 \pm \gamma_5)/2$ are the projection operators.

The SUSY-QCD virtual corrections of the cross section to the subprocesses $q\bar{q}$, gg can be expressed as

$$\hat{\sigma}_{\mathrm{virtual}}^{(q\bar{q},gg)} = \int d(PS_3)\bar{\sum}2\mathrm{Re}(\mathcal{M}_{\mathrm{tree}}^{(q\bar{q},gg)}\mathcal{M}_{\mathrm{virtual}}^{(q\bar{q},gg)\dagger}), \quad (23)$$

where $\mathcal{M}_{\mathrm{tree}}^{(q\bar{q})}$ and $\mathcal{M}_{\mathrm{tree}}^{(gg)}$ are the Born amplitudes for $q\bar{q}$, gg subprocesses, and $\mathcal{M}_{\mathrm{virtual}}^{(q\bar{q})}$ and $\mathcal{M}_{\mathrm{virtual}}^{(gg)}$ are the renormalized amplitudes of all the NLO SUSY-QCD Feynman diagrams involving virtual gluons/quarks and gluinos/squarks for $q\bar{q}$ annihilation and gg fusion processes, respectively. Then the $\hat{\sigma}_{\mathrm{virtual}}$ is UV finite, but still has IR divergence.

B. Real corrections

The real corrections result from processes where an additional massless particle is radiated in the final state. It is possible to radiate either an additional gluon $g(p_6)$ from any initial- or final-state parton in the LO diagrams

$$q(p_1) + \bar{q}(p_2) \to \tilde{t}_1(p_3) + \bar{\tilde{t}}_1(p_4) + h(p_5) + g(p_6),$$
$$g(p_1) + g(p_2) \to \tilde{t}_1(p_3) + \bar{\tilde{t}}_1(p_4) + h(p_5) + g(p_6), \quad (24)$$

or to add an additional final-state quark $q(p_6)$ or antiquark $\bar{q}(p_6)$,

$$(q,\bar{q})(p_1) + g(p_2) \to \tilde{t}_1(p_3) + \bar{\tilde{t}}_1(p_4) + h(p_5) + (q,\bar{q})(p_6). \quad (25)$$

We have extracted both soft and collinear IR singularities by implementing a phase space slicing method with two cutoffs [15]. We introduce an arbitrary small soft cutoff δ_s to separate the phase space into two regions, according to whether the energy of the emitted gluon is soft or hard. Consider the case when parton 6 is a soft gluon. The soft region S is defined in terms of the gluon energy E_6 in the $p_1 + p_2$ rest frame by $0 \le E_6 \le \delta_s\sqrt{s_{12}}/2$. The hard region H is the complement: $E_6 > \delta_s\sqrt{s_{12}}/2$. Furthermore, we introduce an arbitrary small collinear cutoff δ_c to decompose $\hat{\sigma}_{\mathrm{hard}}$ into a sum of hard/collinear HC and hard/noncollinear H$\bar{\mathrm{C}}$ terms to isolate the remaining collinear singularities from $\hat{\sigma}_{\mathrm{hard}}$, i.e.,

$$\hat{\sigma}_{\mathrm{hard}} = \hat{\sigma}_{\mathrm{HC}} + \hat{\sigma}_{\mathrm{H\bar{C}}}. \quad (26)$$

The soft, HC, and H$\bar{\mathrm{C}}$ parts of the cross section all depend on the cutoffs, but their sum is cutoff independent. The partonic real cross section is given by

$$\hat{\sigma}_{\mathrm{real}} = \hat{\sigma}_{\mathrm{soft}} + \hat{\sigma}_{\mathrm{hard}}. \quad (27)$$

In the soft limit, the gluon radiation is described by an eikonal current [16]. For the $q\bar{q}$ collision channel the parton-level soft cross section can be written as

$$\hat{\sigma}_{\mathrm{soft}} = \hat{\sigma}_{\mathrm{LO}} \otimes \frac{\alpha_s}{2\pi}\sum_{i,j=1}^{4}(\mathbf{T}_i \cdot \mathbf{T}_j)g_{ij}(p_i, p_j), \quad (28)$$

where $\mathbf{T}_i$ are the color operators [17,18], and g_{ij} are the soft integrals defined as

$$g_{ij}(p_i, p_j) = \frac{(2\pi\mu)^{2\epsilon}}{2\pi}\int_{E_6 \le \Delta E}\frac{d^{D-1}\mathbf{p_6}}{E_6}\Big[\frac{2(p_i p_j)}{(p_i p_6)(p_j p_6)} - \frac{p_i^2}{(p_i p_6)^2} - \frac{p_j^2}{(p_j p_6)^2}\Big]. \quad (29)$$

Using the definitions of color operators, we get the expressions of $\hat{\sigma}_{\mathrm{soft}}$ [18,19] for the $q\bar{q}$ annihilation channel,

$$\hat{\sigma}_{\mathrm{soft}}^{q\bar{q}} = -\frac{\alpha_s}{2\pi}\Big[\frac{1}{6}(g_{12} + g_{34}) - \frac{7}{6}(g_{13} + g_{24}) - \frac{1}{3}(g_{14} + g_{23})\Big]\hat{\sigma}_{\mathrm{LO}}^{q\bar{q}}, \quad (30)$$

and for the gg collision channel,

$$\hat{\sigma}^{gg}_{\rm soft} = \frac{\alpha_s}{12\pi}\int d\Phi_3 \bar{\sum}\Big[\Big(\frac{256}{3}(9g_{12}+9g_{13}+9g_{24}-g_{34})+96(g_{12}-g_{14}-g_{23}+g_{34})\Big)|\mathcal{M}^{gg}_1|^2 + \Big(\frac{256}{3}(9g_{12}+9g_{23}+9g_{14}-g_{34})+96(g_{12}-g_{13}-g_{24}+g_{34})\Big)|\mathcal{M}^{gg}_2|^2 - 2\Big(\frac{32}{3}(9g_{12}+9g_{13}+9g_{24}-g_{34})-96(g_{12}-g_{14}-g_{23}+g_{34})\Big){\rm Re}(\mathcal{M}^{gg\dagger}_1\mathcal{M}^{gg}_2)\Big], \quad (31)$$

where $\mathcal{M}^{gg}_1$ and $\mathcal{M}^{gg}_2$ have been expressed in Eqs. (7) and (8), respectively.

The contribution from the H$\bar{\rm C}$ region, $\hat{\sigma}_{\rm H\bar{C}}$, is finite, and we compute it numerically by using standard Monte Carlo integration techniques. The H$\bar{\rm C}$ real corrections have been checked using MADGRAPH [20]. In the HC region, the initial-state parton i ($i = q, \bar{q}, g$) is considered to split into a hard parton i' and a collinear gluon g, $i \to i'g$, with $p_{i'} = zp_i$ and $p_6 = (1-z)p_i$. The matrix element squared for $q\bar{q}(gg) \to \tilde{t}_1\bar{\tilde{t}}_1 hg$ factorizes into the Born matrix element squared and the Altarelli-Parisi splitting function for $i \to i'g$, i.e.,

$$\bar{\sum}|\mathcal{M}_{\rm HC}(ij\to\tilde{t}_1\bar{\tilde{t}}_1hg|^2 \overset{\rm collinear}{\to}(4\pi\alpha_s) \times\sum_i\bar{\sum}|\mathcal{M}_{\rm LO}(i'j\to\tilde{t}_1\bar{\tilde{t}}_1h)|^2\frac{2P_{ii'}(z,\epsilon)}{z(2p_i\cdot p_6)}. \quad (32)$$

Using the approximation $p_i - p_6 \simeq zp_i (i = 1, 2)$, the integral over the collinear gluon degrees of freedom can then be performed separately, and this allows us to explicitly extract the collinear singularities of $\hat{\sigma}_{\rm hard}$. $\hat{\sigma}_{\rm HC}$ turns out to be of the form [15,21]

$$\hat{\sigma}_{\rm HC} = \Big[\frac{\alpha_s}{2\pi}\frac{\Gamma(1-\epsilon)}{\Gamma(1-2\epsilon)}\Big(\frac{4\pi\mu^2}{m_t^2}\Big)^\epsilon\Big]\Big(-\frac{1}{\epsilon}\Big)\delta_c^{-\epsilon} \times\int_0^{1-\delta_s}dz\Big[\frac{(1-z)^2}{2z}\frac{s'}{m_t^2}\Big]^{-\epsilon}P_{ii'}(z) \times\hat{\sigma}_{\rm LO}(i'j\to\tilde{t}_1\bar{\tilde{t}}_1h)+(i\leftrightarrow j), \quad (33)$$

where $s' = 2p_{i'}\cdot p_j$. These initial-state collinear divergences are absorbed into the parton distribution functions. In the calculation of the hard light-quark emission subprocesses, we adopt a method similar to that for hard gluon emission.

C. NLO SUSY-QCD corrected cross section

The final result for the NLO QCD corrected cross section is obtained by convoluting the parton cross section with the NLO parton distribution function $\mathcal{F}^p_i(x,\mu)$ ($i = q, g$), thereby absorbing the remaining initial-state singularities into the PDFs. The NLO SUSY-QCD corrections of the total cross sections contributed by $q\bar{q}$ annihilation and gg fusion subprocesses in the initial-state collinear phase space region are obtained as [18,22]

$$\sigma^{qq}_{\rm NLO} = \int dx_1dx_2\mathcal{F}^p_q(x_1,\mu)\mathcal{F}^p_{\bar{q}}(x_2,\mu)[\hat{\sigma}^{qq}_{\rm LO}(x_1,x_2,\mu) + \hat{\sigma}^{qq}_{\rm virtual}(x_1,x_2,\mu)+\hat{\sigma}^{qq}_{\rm soft}(x_1,x_2,\mu)+(1\leftrightarrow2)] + \sigma^{qq}_{\rm HC}+\int dx_1dx_2[\mathcal{F}^p_q(x_1,\mu)\mathcal{F}^p_{\bar{q}}(x_2,\mu) \times\hat{\sigma}^{qq}_{\rm H\bar{C}}(x_1,x_2,\mu)+(1\leftrightarrow2), \quad (34)$$

and the NLO QCD corrected cross-section part for the gg fusion subprocess has the expression

$$\sigma^{gg}_{\rm NLO} = \frac{1}{2}\int dx_1dx_2\mathcal{F}^p_g(x_2,\mu)\mathcal{F}^p_g(x_2,\mu)[\hat{\sigma}^{gg}_{\rm LO}(x_1,x_2,\mu) + \hat{\sigma}^{gg}_{\rm virtual}(x_1,x_2,\mu)+\hat{\sigma}^{gg}_{\rm soft}(x_1,x_2,\mu)+(1\leftrightarrow2)] + \sigma^{gg}_{\rm HC}+\frac{1}{2}\int dx_1dx_2[\mathcal{F}^p_g(x_1,\mu)\mathcal{F}^p_g(x_2,\mu) \times\hat{\sigma}^{gg}_{\rm H\bar{C}}(x_1,x_2,\mu)+(1\leftrightarrow2)]. \quad (35)$$

The cross section of $(q,\bar{q})g \to \tilde{t}_1\bar{\tilde{t}}_1h + (q,\bar{q})$ ($q = u, d$) can be written as

$$\sigma^{qg}_{\rm NLO} = \sigma^{qg}_{\rm HC}+\sum_{i=q,\bar{q}}\int dx_1dx_2[\mathcal{F}^p_i(x_1,\mu)\mathcal{F}^p_g(x_2,\mu) \times\hat{\sigma}^{qg}_{\rm H\bar{C}}(x_1,x_2,\mu)+(1\leftrightarrow2)], \quad (36)$$

with the H$\bar{\rm C}$ partonic cross section given by

$$\hat{\sigma}^{ij}_{\rm H\bar{C}} = \int_{\rm H\bar{C}}\bar{\sum}|M(ij\to\tilde{t}_1\bar{\tilde{t}}_1hg(q,\bar{q}))|^2d(PS_4). \quad (37)$$

Finally, the NLO QCD corrected total cross sections for $pp \to \tilde{t}_1\bar{\tilde{t}}_1h$ can be obtained by using the formula

$$\sigma_{\rm NLO} = \sigma^{qq}_{\rm NLO}+\sigma^{gg}_{\rm NLO}+\sigma^{qg}_{\rm NLO}. \quad (38)$$

IV. NUMERICAL RESULTS AND DISCUSSIONS

A. LO total cross sections

In the following we discuss in detail our results for the LO total cross section for $pp \to \tilde{t}_1\bar{\tilde{t}}_1h$. As a numerical demonstration, we choose the point SPS1a as a benchmark for our numerical study [23]. SPS1a is a typical mSUGRA point with an intermediate value of $\tan\beta = 10$, $\mu > 0$. It has a model line attached to it, which is specified by $M_0 = -A_0 = 100$ GeV and $M_{1/2} = 250$ GeV. Starting from the five mSUGRA parameters M_0, $M_{1/2}$, A_0, $\tan\beta$,

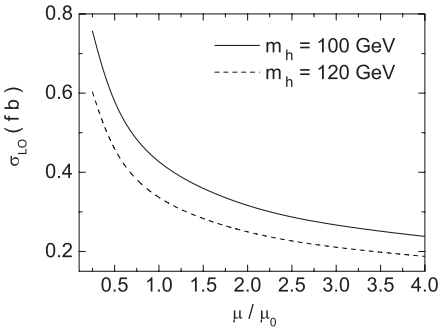

FIG. 3. Variation of the LO cross sections for the $pp \to \tilde{t}_1\bar{\tilde{t}}_1 h$ at the LHC with the renormalization/factorization scale μ.

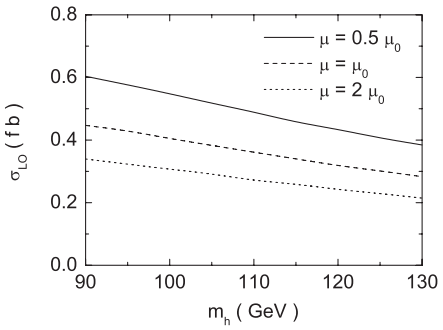

FIG. 4. Variation of the LO cross section for the $pp \to \tilde{t}_1\bar{\tilde{t}}_1 h$ at the LHC with the Higgs boson mass m_h.

and sign(μ), we have generated the spectrum of masses, widths, couplings, and mixings relative to squarks and Higgs particles by running the MSUGRA program contained in the package ISAJET [24], version 7.69. The value of the top mass we used was 175 GeV. Note that typical electroweak parameters, such as $\alpha_{\rm em}$ and $\sin^2\theta_W$, were also taken from this program, as they enter the renormalization group equations of the SUSY theory. The stop masses in this scenario are given by $m_{\tilde{t}_1} = 377.39$ GeV and $m_{\tilde{t}_2} = 571.62$ GeV. The numerical analyses of the hadronic cross

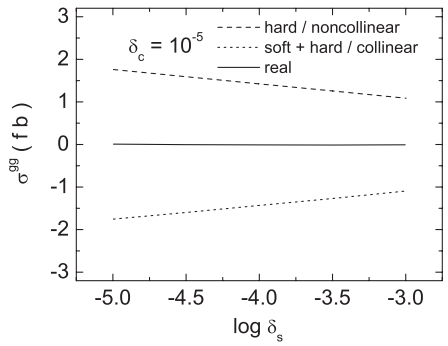

FIG. 5. Dependence of $\sigma^{gg}_{\rm soft} + \sigma^{gg}_{\rm HC}$, $\sigma^{gg}_{\rm H\bar{C}}$ and their sum (real) on the soft cutoff δ_s for $m_h = 120$ GeV and $\mu = \mu_0$.

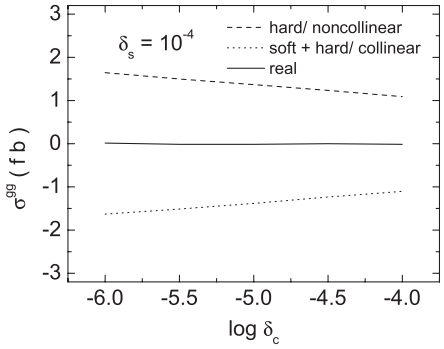

FIG. 6. Dependence of $\sigma^{gg}_{\rm soft} + \sigma^{gg}_{\rm HC}$, $\sigma^{gg}_{\rm H\bar{C}}$ and their sum (real) on the collinear cutoff δ_c for $m_h = 120$ GeV and $\mu = \mu_0$.

sections have been performed for the CERN LHC with a pp center of mass of $\sqrt{s} = 14$ TeV. The hadronic cross sections are obtained by convoluting the partonic cross sections with the parton distribution functions of the initial-state hadrons as specified in Eq. (14). The LO numerical results are based on the one-loop evolution of α_s and the CTEQ6L1 PDFs [25]. By default, we set the renormalization scale μ_R and the factorization scale μ_F to the common renormalization/factorization scale μ.

Figure 3 shows the total LO cross sections as a function of the renormalization/factorization scale for $m_h = 100$ GeV and 120 GeV. The renormalization/factorization scale dependence of the LO cross-section prediction is indicated by bands resulting from varying the central scale $\mu_0 = m_{\tilde{t}_1} + \frac{m_h}{2}$ up and down by a factor 2. The variation of the scale shows that the LO prediction for the total cross section is plagued by scale uncertainty of about 44% and therefore cannot provide a reliable prediction. This underlines the need for NLO. Figure 4 shows the dependence of the total LO cross section on the Higgs mass. For the Higgs mass between 90 GeV and 130 GeV, the cross section varies between about 0.4468 fb and 0.283 fb, if the central scale μ_0 is chosen for the renormalization and factorization scales. For $\mu = 0.5\mu_0$, the cross section increases and varies between about 0.6036 fb and 0.3843 fb.

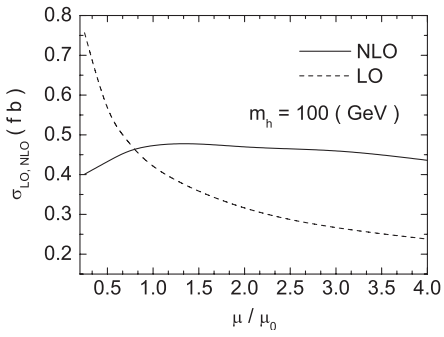

FIG. 7. The total cross sections $\sigma_{\rm LO}$ and $\sigma_{\rm NLO}$ for the process $pp \to \tilde{t}_1\bar{\tilde{t}}_1 h$ as functions of the renormalization/factorization scale with $m_h = 100$ GeV.

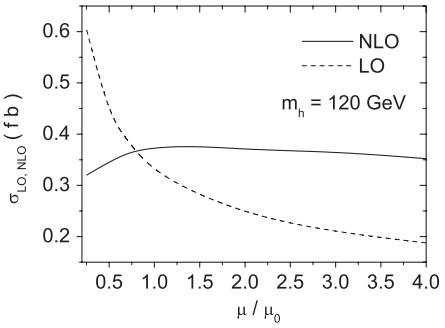

FIG. 8. The total cross sections $\sigma_{\rm LO}$ and $\sigma_{\rm NLO}$ for the process $pp \to \tilde{t}_1\bar{\tilde{t}}_1 h$ as functions of the renormalization/factorization scale with $m_h = 120$ GeV.

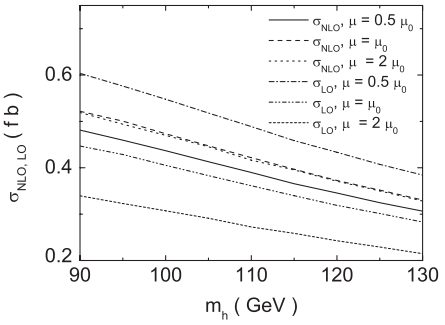

FIG. 9. LO and NLO total cross sections for $pp \to \tilde{t}_1\bar{\tilde{t}}_1 h$ with the renormalization/factorization scale set to $\mu = 0.5\mu_0$, $\mu = \mu_0$, and $\mu = 2\mu_0$ as a function of m_h.

But for $\mu = 2\mu_0$, the cross section decreases and varies between about 0.3394 fb and 0.2146 fb.

B. Total NLO SUSY-QCD corrected cross sections

In our numerical calculation, we adopt the CTEQ6M PDFs [25] and the two-loop evolution of α_s to evaluate the hadronic NLO SUSY-QCD corrected cross section. Figures 5 and 6 show the cancellation of the δ_s and δ_c dependence between $\sigma^{gg}_{\rm soft} + \sigma^{gg}_{\rm HC}$ and $\sigma^{gg}_{\rm H\bar{C}}$, respectively, for gg fusion. Similar plots could be obtained for the other subprocess, $q\bar{q}$.

In Figs. 7 and 8 we show the renormalization/factorization scale dependence of the LO and NLO total cross sections. We observe a significant reduction of the renormalization/factorization scale dependence and the stabilization of the theoretical predictions for the cross section upon going from LO to NLO. We estimate the size of the remaining scale uncertainties to be about 10% at NLO when the central scale is varied up and down by a factor of 2.

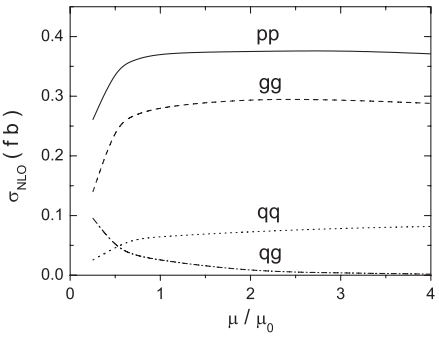

FIG. 10. Total cross section for $pp \to \tilde{t}_1\bar{\tilde{t}}_1 h$ and partonic cross sections at the LHC in the NLO approximation, as functions of the renormalization/factorization scale with $m_h = 120$ GeV.

In Fig. 9 we depict the LO and NLO total cross sections with the renormalization/factorization scale set to $\mu = 0.5\mu_0$, $\mu = \mu_0$, and $\mu = 2\mu_0$ as a function of m_h.

Figure 10 demonstrates that the main contributions are coming from the subprocess $gg \to \tilde{t}_1\bar{\tilde{t}}_1 h$, which receives positive NLO corrections in the domain of the central renormalization/factorization scale. For the hard collinear quark emission (qg), the NLO SUSY-QCD corrections are small.

V. CONCLUSIONS

In this paper we have calculated the NLO SUSY-QCD corrections to the production of neutral Higgs bosons in association with a lower mass stop quark pair at the LHC in the MSSM assuming a mSUGRA symmetry breaking scheme. Our interest in such a reaction comes from the fact that it constitutes a production mechanism of Higgs bosons and also because it carries a strong dependence on the five inputs of the SUSY model, so that it can possibly be used to constrain the latter.

We have analyzed the dependence of the NLO SUSY-QCD corrected cross section on the renormalization/factorization scale and Higgs boson mass. We have found that the NLO SUSY-QCD corrections significantly reduce the dependence of the total cross section on the renormalization/factorization scale. This then reduces the theoretical uncertainty of the cross section from 44% at LO to 10% at NLO when the renormalization/factorization scale is varied between half and twice the central scale.

[1] S. L. Glashow, Nucl. Phys. **22**, 579 (1961); S. Weinberg, Phys. Rev. Lett. **19**, 1264 (1967); A. Salam, in *Proceedings of the 8th Nobel Symposium, Stockholm, 1968*, edited by N. Svartholm (Almqvist and Wiksells, Stockholm, 1968), p. 367; S. L. Glashow, J. Iliopoulos, and L. Maiani, Phys. Rev. D **2**, 1285 (1970); H. Fritzsch,

M. Gell-Mann, and H. Leutwyler, Phys. Lett. 47B, 365 (1973); E. S. Abers and B. W. Lee, Phys. Rep. **9**, 1 (1973); S. F. Novaes, arXiv:hep-ph/0001283.
[2] H. P. Nilles, Phys. Rep. **110**, 1 (1984); H. E. Haber and G. L. Kane, Phys. Rep. **117**, 75 (1985).
[3] J. F. Gunion and H. E. Haber, Nucl. Phys. **B272**, 1 (1986).
[4] J. Ellis and S. Rudaz, Phys. Lett. **128B**, 248 (1983).
[5] K. Nakamura *et al.* (Particle Data Group), J. Phys. G **37**, 075021 (2010).
[6] A. Djouadi, J. L. Kneur, and G. Moultaka, Phys. Rev. Lett. **80**, 1830 (1998).
[7] G. Bélanger *et al.*, Eur. Phys. J. C **9**, 511 (1999).
[8] A. Dedes and S. Moretti, Phys. Rev. D **60**, 015007 (1999).
[9] A. Dedes and S. Moretti, Eur. Phys. J. C **10**, 515 (1999).
[10] J. Küblbeck, M. Böhm, and A. Denner, Comput. Phys. Commun. **60**, 165 (1990).
[11] G. J. Van Oldenborgh and J. A. M. Vermaseren, Z. Phys. C **46**, 425 (1990).
[12] G. 't Hooft, Nucl. Phys. **B35**, 167 (1971).
[13] G. Passarino and M. Veltman, Nucl. Phys. **B160**, 151 (1979).
[14] G. J. van Oldenborg, Comput. Phys. Commun. **66**, 1 (1991).
[15] B. W. Harris and J. F. Owens, Phys. Rev. D **65**, 094032 (2002).
[16] R. J. Glauber,*Lectures in Theoretical Physics*, edited by W. E. Brittin and L. G. Dunham (Inter Science Publishers, New York, 1959), Vol. I; H. D. I. Abarbanel and C. Itzykson, Phys. Rev. Lett. **23**, 53 (1969); E. Kujawski, Phys. Rev. D**4**, 2573 (1971); W. Tobocman and M. Pauli, Phys. Rev. D **5**, 2088 (1972); M. Obu, Prog. Theor. Phys. **50**, 147 (1973); C. J. Joachain and C. Quigg, Rev. Mod. Phys. **46**, 279 (1974); J. P. Harnad, Ann. Phys. (N.Y.) **91**, 413 (1975); Q. Bui-Duy, Phys. Rev. D **11**, 1635 (1975); T. Ishihara, Prog. Theor. Phys. **54**, 1106 (1975); T. W. Chen and D. W. Hoock, Phys. Rev. D **12**, 1765 (1975); F. Guerin and H. M. Fried, Phys. Rev. D **33**, 3039 (1986); L. Gamberg and K. A. Milton, Phys. Rev. D **61**, 075013 (2000).
[17] W. Beenakker, S. Dittmaier, M. Kramer, B. Plumper, M. Spira, and P. M. Zerwas, Phys. Rev. Lett. **87**, 201805 (2001).
[18] Wu Peng *et al.*, Phys. Rev. D **73**, 015012 (2006).
[19] W. Beenakker, S. Dittmaier, M. Kramer, B. Plümper, M. Spira, and P. M. Zerwas, Nucl. Phys. **B653**, 151 (2003).
[20] T. Stelzer and W. F. Long, Comput. Phys. Commun. **81**, 357 (1994).
[21] U. Baur, S. Keller, and D. Wackeroth, Phys. Rev. D **59**, 013002 (1998).
[22] L. Reina, S. Dawson, and D. Wackeroth, Phys. Rev. D **65**, 053017 (2002).
[23] B. C. Allanach *et al.*, Eur. Phys. J. C **25**, 113 (2002).
[24] H. Baer *et al.*, arXiv:hep-ph/0312045.
[25] J. Pumplin, D. R. Stump, J. Huston, H. L. Lai, P. Nadolsky, and W. K. Tung, J. High Energy Phys. 07 (2002) 012; H. L. Lai *et al.*, Eur. Phys. J. C **12**, 375 (2000).